Shape and superdeformed structure in Hg isotopes in relativistic mean field model

S. K. Patra, S. Yoshida,* and N. Takigawa
Department of Physics, Faculty of Science, Tohoku University, 980-77 Sendai, Japan

C. R. Praharaj
Institute of Physics, Bhubaneswar-751 005, India
(Received 23 March 1994)

Various shapes of Hg isotopes are calculated using a relativistic mean field theory. We observe shape transitions from oblate to prolate and prolate to oblate at $A = 178$ and $A = 188$, respectively. Both in the oblate and in the prolate solutions the sign of the hexadecupole moment changes from positive to negative values with increasing mass number. The predicted shape of the ground state agrees with the available data contrary to nonrelativistic calculations for neutron-deficient isotopes. A low-lying superdeformed configuration is found in some isotopes, and found to be the ground state for ^{180}Hg. A possible discrepancy between the experimental data of the quadrupole deformation and those of the charge radii is pointed out.

PACS number(s): 21.60.−n, 21.10.Ft, 21.30.+y, 27.70.+q

I. INTRODUCTION

The change of the shape of rare-earth nuclei and of other properties of nuclear structure with neutron number has attracted much theoretical and experimental attention for many years [1–5]. Another interesting feature is shape isomerism, i.e., shape coexistence, where states with different deformations appear with nearly equal energy [6–8]. Light mercury isotopes far from the stability line provide a classic example of the existence of bands of levels built on a well-deformed and a nearly spherical shape [6,9]. Similar shape coexistence is observed more frequently in the $Z \approx 80$ region. The existence of superdeformed bands is an extreme of shape isomerism.

It is a challenging theoretical problem to understand the origin of the shape isomerism. Secondary minima and shape transitions along the isotope chain have been found for Hg isotopes within the framework of non-relativistic Hartree-Fock (HF) calculations [10]. Bonche *et al.* [11,12] performed HF calculations including a BCS pairing correlation and showed that the shape isomerism appears not only in Hg isotopes, but also in other rare-earth nuclei. The location of the shape isomers over a wide range of nuclei has been discussed also by macroscopic-microscopic calculations of the potential energy surface (PES) as a function of the deformation parameter [7,13]. A drawback of these nonrelativistic calculations is that the input, such as the parameters of the Skyrme interaction, was determined phenomenologically in order to reproduce the properties of stable nuclei. Therefore, it is not clear whether one can extend them to studying nuclei far from the β stability line. Another problem is that the available model space in practical calculations is too small to discuss superdeformed states. Also, as we point out later, they cannot reproduce some of the existing data.

Relativistic mean field (RMF) models are free from the first two difficulties of nonrelativistic calculations mentioned above. A distinct advantage is that, with proper relativistic kinematics and with the mesons and their properties already known or fixed from the properties of a small number of finite nuclei [14], the method gives excellent results for the binding energies, root mean square (rms) radii, quadrupole and hexadecupole deformations, and other nuclear properties not only of spherical nuclei, but also of well known deformed nuclei [14–20]. It explains the change of shapes along the Pt [15] and Ho isotope chains [16] very well. The same parameter sets also well describe the nuclear matter properties. One of the major attractive features of the RMF approach is that the spin-orbit interaction and the associated nuclear shell structure naturally arise from meson-nucleon interaction [14,19,20]. The inclusion of the ρ meson takes care of the neutron-proton asymmetry. We can thus expect that the RMF calculations provide useful information about the structure of nuclei far from the stability line including those near the neutron and the proton drip lines. Also, since the RMF approach is not limited to small model space, one can apply it to studying superdeformed structures, which involve large j orbits of high-lying shells.

Many theoretical as well as experimental papers have recently focused their interest on the shape transition [9], shape isomerism, and the observation of superdeformed bands [21] in neutron-deficient Hg isotopes. It is thus of great interest to explore in detail the structures of these nuclei and also to look for possible shape isomerism based on the RMF formalism.

The paper is organized as follows. In Sec. II we present

*Electronic address: yoshida@nucl.phys.tohoku.ac.jp

the equations and the procedure of numerical calculations. The results for binding energies, quadrupole deformation, hexadecupole moments, and rms radii for both prolate and oblate solutions as well as superdeformed states are discussed in Sec. III. A summary and concluding remarks are given in Sec. IV.

II. THEORY AND CALCULATION

The relativistic mean field model uses a Lagrangian density for the interacting nucleon-meson many-body system [14,17–20], consisting of nucleons, scalar (σ) and vector mesons ($\omega, \vec{\rho}$) and photon.

$$\begin{aligned}\mathcal{L} = {} & \overline{\psi_i}\{i\gamma^\mu\partial_\mu - M\}\psi_i + \tfrac{1}{2}\partial^\mu\sigma\partial_\mu\sigma - U(\sigma) - g_s\overline{\psi_i}\psi_i\sigma - \tfrac{1}{4}\Omega^{\mu\nu}\Omega_{\mu\nu} \\ & + \tfrac{1}{2}m_\omega^2 V^\mu V_\mu - g_\omega\overline{\psi}_i\gamma^\mu\psi_i V_\mu - \tfrac{1}{4}\vec{B}^{\mu\nu}\cdot\vec{B}_{\mu\nu} + \tfrac{1}{2}m_\rho^2\vec{\rho}^\mu\cdot\vec{\rho}_\mu \\ & - g_\rho\overline{\psi}_i\gamma^\mu\vec{\tau}\psi_i\cdot\vec{\rho}_\mu - \tfrac{1}{4}F^{\mu\nu}F_{\mu\nu} - e\overline{\psi}_i\gamma^\mu\frac{(1-\tau_{3i})}{2}\psi_i A_\mu. \end{aligned} \tag{2.1}$$

The scalar meson is assumed to move in a nonlinear potential [22]

$$U(\sigma) = \tfrac{1}{2}m_\sigma^2\sigma^2 + \tfrac{1}{3}g_2\sigma^3 + \tfrac{1}{4}g_3\sigma^4. \tag{2.2}$$

In Eq. (2.1) ψ_i are the Dirac spinors for nucleons, whose third component of the isospin is denoted by τ_{3i}. The g_s, g_ω, g_ρ, and $\frac{e^2}{4\pi} = \frac{1}{137}$ are the coupling constants for σ, ω, and ρ mesons and the photon, respectively. M is the nucleon mass, and m_σ, m_ω, and m_ρ are the masses of the σ, ω, and ρ mesons, respectively. $\Omega^{\mu\nu}$, $\vec{B}^{\mu\nu}$, and $F^{\mu\nu}$ are the field tensors for the V^μ, $\vec{\rho}^\mu$ and the photon fields, respectively [14,17–20].

We need a static solution of the above Lagrangian in order to describe the ground state properties. In this case the meson and the electromagnetic fields are assumed to be time independent, whereas the nucleon wave functions oscillate with a single particle energy ϵ_i. The equations for the fermion and the boson fields [14,17–20] are obtained from the Lagrangian given by Eq. (2.1) and can be found in Refs. [14,17–20]. They are nonlinear coupled partial differential equations, which are solved self-consistently by iteration.

Practically, these equations are solved by expanding the upper and the lower components $f_i^\pm$ and $g_i^\pm$ of the Dirac spinor ψ_i and the wave functions of the boson fields in terms of deformed harmonic oscillator bases, taking volume conservation into account [17]. The frequencies $\hbar\omega_\perp$ and $\hbar\omega_z$ of the harmonic oscillator potential are related to the quadrupole deformation parameter β_0 [17].

In numerical calculations we truncate the harmonic oscillator bases at the maximum oscillator quanta $N_{\max} = 12$ for both bosons and fermions. The deformation parameter β is obtained from the calculated quadrupole moments for the protons and the neutrons through

$$Q = Q_n + Q_p = \sqrt{\frac{9}{5\pi}}AR^2\beta, \tag{2.3}$$

and the hexadecupole moment is defined by

$$Q_4^{n,p} = \langle r^4 Y_{40}(\theta)\rangle_{n,p}, \tag{2.4}$$

where $R = 1.2A^{1/3}$. The total hexadecupole moment is obtained by summing Q_4^n and Q_4^p. If we denote the radius of the proton distribution by r_p, the charge radius is given by $r_{ch} = \sqrt{r_p^2 + 0.64}$ fm by taking the finite size of the proton into account. The total binding energy of the system is given by $-E_{\text{total}}$, where

$$E_{\text{total}} = E_{\text{part}} + E_\sigma + E_\omega + E_\rho + E_C + E_{\text{pair}} + E_{\text{c.m.}}. \tag{2.5}$$

The E_{part} is the sum of single-particle energies of the nucleons and E_σ, E_ω, E_ρ, E_C, and E_{pair} are the contributions from the meson fields, the Coulomb field and the pairing energy, respectively. We used the same pairing gap as in Ref. [23]. $E_{\text{c.m.}} = -\frac{3}{4}\times 41A^{-\frac{1}{3}}$ is a nonrelativistic approximation to correct the energy of the center-of-mass motion.

The set of coupled equations for nucleons and bosons is solved iteratively following the procedure of Ref. [17] using the nonlinear parameter set (NL1) [14] (M = 938.0, m_σ = 492.25, m_ω = 795.359, and m_ρ = 763.0 MeV, g_σ = 10.138, g_ω = 13.285, g_ρ = 4.9755, g_2 = -12.172 fm^{-1}, $g_3 = -36.265$).

III. RESULTS AND DISCUSSIONS

We calculate the binding energies, the rms radii of the proton and the neutron distributions, and the quadrupole and the hexadecupole moments for Hg isotopes with the neutron number N = 90–120. The results for the quadrupole deformation parameters β and the binding energies are listed in Table I for various prolate and oblate solutions. The experimental binding energies [24] and quadrupole deformation parameters, as well as the quadrupole deformation parameters calculated by other theoretical methods, are also given for comparison, wherever possible. Our theoretical binding energies and β values agree fairly well with the experimental values.

Experimentally, heavy Hg isotopes are known to be oblate in shape with a moderate magnitude of the quadrupole deformation [25]. In Fig. 1, we plot the difference of the binding energies for the oblate and the prolate solutions for a wide range of Hg isotopes. For a given

nucleus the solution with the maximum binding energy gives the ground state and the other solution corresponds to an intrinsic excited state. The figure indicates that the shape of heavy Hg isotopes is indeed oblate. Figure 1 and Table I show, however, that the normal prolate solution has lower energy than the oblate solution for ^{178,180,182,184,186}Hg. In contrast, nonrelativistic potential energy surface (PES), HF, and the HF+BCS [7,8,10,12] calculations predict these isotopes to be oblate. The difference of the binding energies for the prolate and the oblate solutions is very small for ^{182}Hg, so that one needs more detailed studies in order to predict the actual shape.

TABLE I. The results of RMF calculations for the binding energies (BE), the rms charge radii, and the quadrupole deformation parameter are compared with experimental data and other theoretical calculations, wherever available. The experimental binding energies and the β values were taken from Refs. [24] and [29,30], respectively. The results of the HF+BCS calculations are from Refs. [8,11] and the potential energy surface (PES) results from Ref. [7]. The binding energies are in MeV and the radii are in fm.

A	BE(RMF)	BE(Expt)	$\beta_{\rm RMF}$	$\beta_{\rm PES}$	$\beta_{\rm HF+BCS}$	$\lvert\beta_{\rm expt.}\rvert$	$r_{\rm ch}$
170	1322.481		−0.021				5.326
	1321.688		0.032				5.327
	1317.536		0.704				5.682
172	1343.888		−0.072				5.341
	1343.565		0.049				5.343
	1339.229		0.679				5.677
174	1363.232	1349.320	−0.039				5.356
	1362.205		0.065				5.356
	1361.044		0.678				5.699
176	1384.051	1369.760	−0.075				5.370
	1382.816		0.279				5.428
	1383.416		0.620				5.659
178	1402.786	1390.428	−0.150	−0.10			5.395
	1404.453		0.314	0.21			5.458
	1403.025		0.594				5.654
180	1421.847	1410.440	−0.327	−0.11	−0.166		5.503
	1422.597		0.334	0.25	0.291		5.481
	1423.446		0.578				5.653
182	1443.328	1430.670	−0.217	−0.12		0.17	5.443
	1443.268		0.339	0.25			5.497
	1442.522		0.567				5.657
184	1459.026	1448.710	−0.230	−0.12	−0.183	0.16	5.458
	1460.467		0.327	0.24	0.286		5.506
	1457.326		0.604				5.703
186	1476.652	1467.130	−0.214	−0.13	−0.188	0.24	5.463
	1477.593		0.289	0.22	0.276		5.495
	1474.050		0.652				5.750
188	1493.202	1485.050	−0.171	−0.13	−0.187	0.14	5.454
	1492.899		0.280	0.21	0.270		5.506
	1491.164		0.682				5.784
190	1508.787	1502.370	−0.173	−0.12	−0.180	0.15	5.465
	1508.200		0.266		0.104		5.513
	1507.828		0.698				5.809
192	1524.686	1519.430	−0.160	−0.12	−0.164	0.14	5.473
	1522.989		0.253		0.098		5.479
	1522.825		0.678		0.53		5.805
194	1540.713	1535.496	−0.140	−0.12		0.13	5.481
	1538.206		0.124				5.464
	1534.518		0.655		0.54		5.795
196	1555.203	1551.235	−0.142	−0.11		0.12	5.489
	1553.668		0.106				5.460
	1548.572		0.595		0.52		5.806
198	1569.169	1566.504	−0.122	−0.09		0.11	5.494
	1567.810		0.084				5.488
	1560.306		0.587		0.51		5.773
200	1581.731	1581.197	−0.097	−0.0	−0.125	0.098	5.498
	1580.577		0.039				5.493
	1572.186		0.619		0.51		5.820

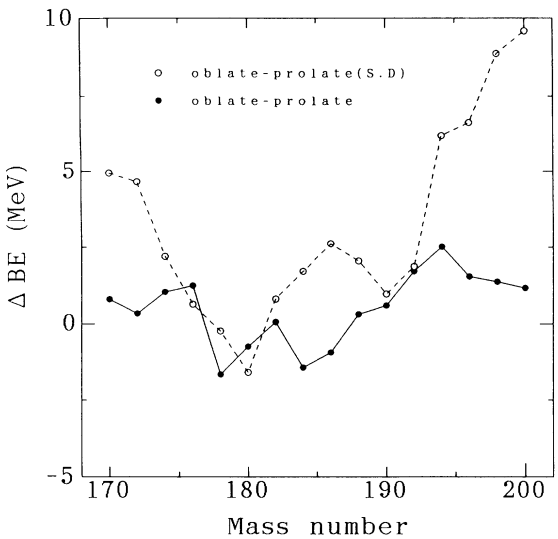

FIG. 1. The difference of the binding energies between the oblate normal and the prolate normal configurations (the filled circles) and between the oblate normal and the prolate superdeformed (SD) configurations (open circles).

In Fig. 2 we compare our results with those of the nonrelativistic macroscopic-microscopic (MM) [23], PES, and HF+BCS calculations [7,8]. There is no shape transition in the MM and the PES calculations. Like our RMF calculations, nonrelativistic Hartree-Fock plus BCS calculations [8,10,12] show shape transitions. However, Fig. 2 shows that the nature of the prolate-oblate shape transition is opposite in the relativistic and in the nonrelativistic calculations. Fig. 2 contains also experimental data. The sign of the deformation parameter is known experimentally too for the heavy isotopes [30]. We notice that the experimental deformation parameters for these nuclei agree very well with our calculations in both sign and magnitude, whereas nonrelativistic Hartree-Fock plus BCS calculations largely deviate from the data. For lighter isotopes ^{182,184,186}Hg we have assumed the same sign for the experimental β value as that in the results of RMF calculations. The agreement between the data [30] and our calculations is then fairly good including the magnitude as we see in Fig. 2. The authors of Ref. [9] measured the quadrupole moment of odd Hg isotopes, and reported a change of the sign of the quadrupole moment at $A \approx 187$. This agrees with our calculations.

We found a low-lying prolate superdeformed configuration in many of the Hg isotopes. They are quite comparable with those predicted by nonrelativistic HF [10] and HF+BCS [11,12] calculations (see Table I). The superdeformed states have been already found for ^{190,192,194}Hg isotopes [26]. Figure 1 indicates that the superdeformed configuration has the highest energy among the three solutions, i.e., the oblate, the prolate, and the superdeformed solutions, for almost all the isotopes. However, it has the largest binding energy for ^{180}Hg, and forms the ground state. In ^{176}Hg it appears in between the oblate and the prolate solutions.

The hexadecupole moment is an interesting quantity in itself. Also, it is becoming clear that the hexadecupole moment strongly influences the fusion cross section in heavy ion collisions at energies below the Coulomb barrier [27,28]. In Fig. 3 we show the hexadecupole mo-

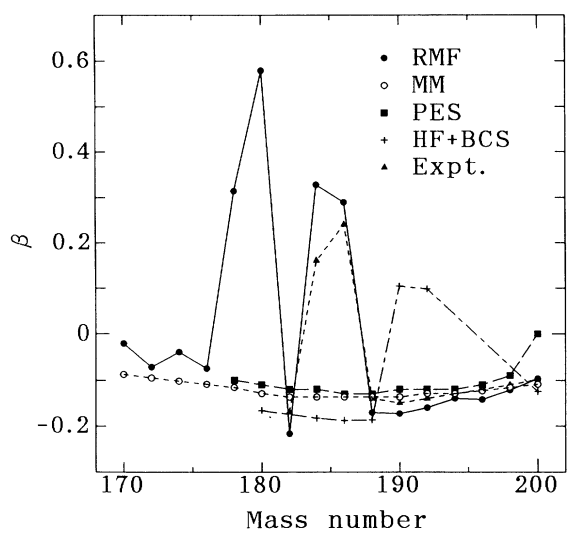

FIG. 2. The quadrupole deformation parameter as a function of the mass number for Hg isotopes. The experimental data [29,30] (the filled triangles) are compared with the results of various theoretical calculations: RMF theory (filled circles), macroscopic-microscopic (MM) calculations [23] (open circles), calculations of the potential energy surface (PES) [7] (filled squares), and HF+BCS calculations [8,11,12] (crosses).

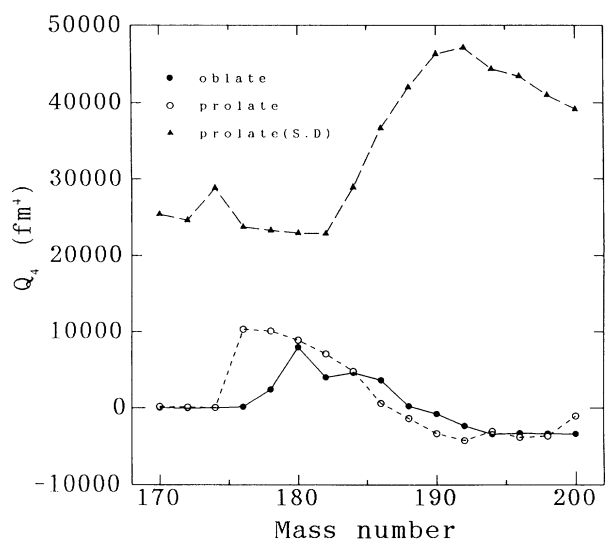

FIG. 3. Hexadecupole moment Q_4 as a function of the mass number for Hg isotopes. The filled circles, the open circles, and the filled triangles are for the oblate normal, the prolate normal, and the prolate superdeformed (SD) configurations, respectively.

ment (Q_4) for the oblate (solid line with filled circles) and the prolate (dashed line with open circles) and for the superdeformed (the dashed line with filled triangles) solutions as a function of the mass number. We find a change in sign from negative to positive for the oblate normal solution around the mass number $A = 176$ and from positive to negative value at mass number $A = 188$. This change in sign of the hexadecupole moment is similar in trend to that in nonrelativistic HF+BCS [8] calculations. The hexadecupole moment of the prolate normal solution increases with increasing mass number. It takes a maximum at $A = 176$ and then decreases. The sign of the hexadecupole moment in the prolate normal solution changes from positive to negative at $A = 188$ in our calculations, whereas the sign changes at $A = 184$ in the HF+BCS calculations. There is no sign change in the macroscopic-microscopic calculations of Moeller *et al.* [23]. The hexadecupole moments for superdeformed configurations are considerably larger than those for prolate and oblate normal solutions. The maximum Q_4 value for the superdeformed configuration is found at $A = 192$.

The charge radii calculated by the RMF and the nonrelativistic HF+BCS theories are plotted in Fig. 4 for both the prolate and the oblate solutions. We find reasonable agreement between the two calculations. In Fig. 5 the rms charge radii in the ground states calculated in the RMF theory are compared with experimental data [29,30] and those in the HF calculations. Figure 5 shows that our RMF results are closer to the experimental values than are the nonrelativistic HF calculations. The charge radii calculated by the RMF theory suddenly increase for ^{184,186}Hg as we reduce the number of neutrons. This contrasts with the experimental data, where the charge radius monotonically decreases including these isotopes. The large charge radius for these isotopes in our RMF calculations is related to the large quadrupole deformation in these nuclei (see Fig. 5). Since this agrees with the experimental data of the quadrupole deformation, a puzzle is then why the charge radius does not reflect this behavior of the quadrupole deformation. In this sense, it looks as if the data of the quadrupole deformation and those of the charge radius are not consistent.

If the data were correct, a possibility to resolve the discrepancy between the experimental data and the present

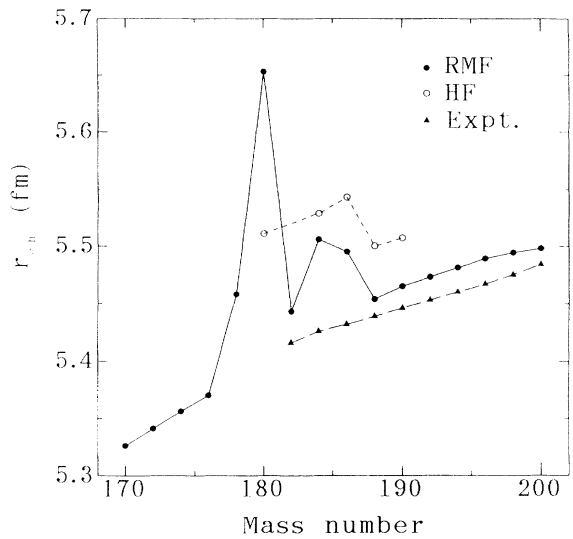

FIG. 5. The charge radii of the ground states of Hg isotopes calculated by the RMF theory are compared with experimental data [29] and the results of nonrelativistic HF calculations [10].

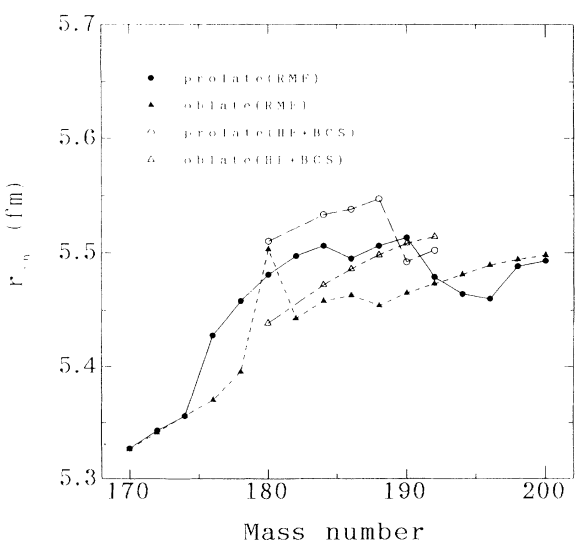

FIG. 4. The charge radii calculated by the RMF theory and the nonrelativistic HF+BCS theory [8] are compared for the prolate and the oblate solutions.

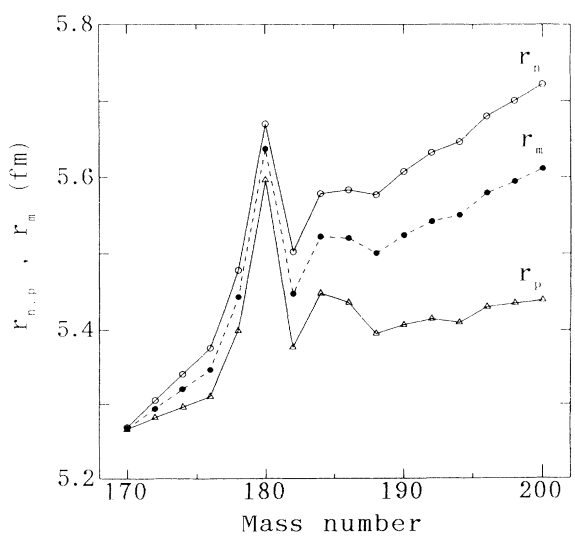

FIG. 6. The rms radii of the proton, the neutron, and the matter distributions as functions of the mass number for Hg isotopes.

theoretical results for the charge radii for ^{184,186}Hg is the shape admixture in the ground state in these nuclei. In fact, the rather short lifetime of the states in the excited band built on the $J^\pi=0^+$ state at excitation energy $E^* = 0.375$ MeV and $E^* = 0.523$ MeV in ^{184}Hg and ^{186}Hg [31], respectively, indicates a sizable admixture of the ground and the excited bands in these nuclei. In order to tackle this problem theoretically, we need to extend our theory to include the angular momentum projection. We also need to refine the theory in order to get better agreement with the experimental data concerning the energy splitting between the two configurations with different shapes. The present theory gives too large a splitting between them. These problems will be reported in forthcoming papers.

In Fig. 6, we plot the rms radii of the proton, and the neutron and the matter distributions in the ground states. We find an anomaly of the rms radius at $A = 180$. This anomaly is related to the fact that the superdeformed state is the ground state in this nucleus.

Table II shows the occupied Nilsson orbits in the prolate normal and the prolate superdeformation configurations of ^{190}Hg. Each orbit is denoted by the Nilsson quantum numbers $[Nn_3\Lambda]$. Only high-lying states whose principal quantum number N is larger than 4 are included in the table. The index nil means unoccupied orbits. It is clear from the table that the occupation of nucleons in the normal and the superdeformed states is very different. For example, some of the Nilsson orbits such as [660] with small Ω values occupied in the superdeformed state are empty in the prolate normal state. On the other hand, some of the large Ω orbits occupied in the normal prolate state are empty in the superdeformed prolate state.

The density distributions for the prolate normal, the oblate normal, and the prolate superdeformed configurations in ^{190}Hg are plotted in Figs. 7(a), 7(b), and 7(c),

TABLE II. High-lying occupied Nilsson orbits for the prolate normal and the prolate superdeformed (SD) solutions of ^{190}Hg.

Occupation	Neutron orbit	Proton orbit
SD (prolate)		
$\frac{1}{2}^+$	[660]	[660]
	[651]	[651]
	[640]	
$\frac{1}{2}^-$	[770]	[7..]nil
$\frac{3}{2}^+$	[651]	[6..]nil
	[642]	
$\frac{3}{2}^-$	[761]	[7..]nil
$\frac{7}{2}^+$	[413]	[413]
	[404]	
	[633]	
$\frac{9}{2}^+$	[404]	[404]
$\frac{9}{2}^-$	[514]	[5..]nil
Normal (prolate)		
$\frac{1}{2}^+$	[640]	[6..]nil
$\frac{1}{2}^-$	[7..]nil	[7..]nil
$\frac{3}{2}^+$	[651]	[6..]nil
$\frac{3}{2}^-$	[7..]nil	[7..]nil
$\frac{7}{2}^+$	[413]	[413]
	[404]	[404]
	[633]	
$\frac{9}{2}^+$	[404]	[404]
	[624]	
$\frac{9}{2}^-$	[514]	[514]

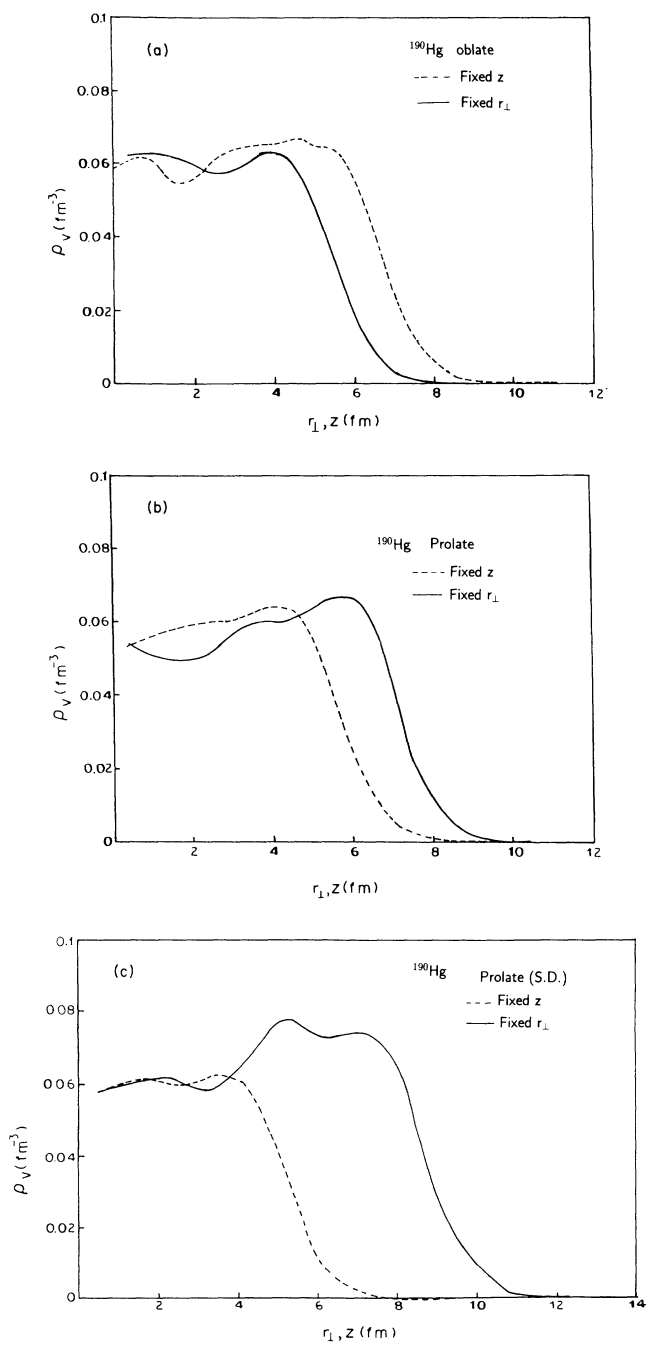

FIG. 7. The density distributions for the oblate normal (a), the prolate normal (b), and the prolate superdeformed configurations (c). The solid and the dashed lines are the density distributions along the z and the perpendicular axes for fixed values of $r_\perp$ and z, respectively.

respectively. We observe in these figures a large difference in the density distribution for the three shapes. The density distributions for the prolate and the oblate normal states are much more compact than that in the superdeformed configuration. In the case of the prolate normal state, the density becomes very small at about 10 fm, whereas for the superdeformed configuration it is elongated up to 12 fm (see Fig. 7).

IV. SUMMARY AND CONCLUSIONS

Three different shapes were predicted in RMF calculations for all the Hg isotopes studied in this paper. In most of them, the oblate solution is found to be the ground state configuration. We found the transitions from oblate to prolate shapes at $A = 178$ and prolate to oblate shapes at $A = 188$. Also we predicted the change of sign of the Q_4 moment from positive to negative value both for the prolate and the oblate solutions with increasing mass number.

The superdeformed configurations were found to be low lying in energy for $A = 170$–192, whereas, for $A > 192$, they appear at rather high excitation energies. The superdeformed state was predicted to be the ground state for ^{180}Hg. In this nucleus, we also found that the prolate normal configuration is located at a fairly low excitation energy. It would be very interesting to experimentally confirm the appearance of the superdeformed ground state in ^{180}Hg. Since this is predicted only in the RMF calculations, such experimental studies will be very useful to assess the power of the RMF calculations.

In the course of our studies, we also found the following. The superdeformed configuration of all the Hg isotopes has a very large hexadecupole moment. We found an anomaly in the charge radius at $A = 180$. This is associated with the superdeformed configuration in the ground state of this nucleus. The general trend of the charge radius calculated by our RMF theory deviates from the existing data for $A = 184$ and 186. Further theoretical as well as experimental studies are desired to resolve this discrepancy.

ACKNOWLEDGMENTS

The authors are grateful to Dr. T. Shinozuka for useful discussions. One of the authors (S.K.P.) is grateful to the Japanese Government for financial support. This work is supported by a Grant-in-Aid for General Scientific Research, Contract No. 06640368, from the Japanese Ministry of Education. Science and Culture.

[1] P. Quentin and H. Flocard, Annu. Rev. Nucl. Part. Sci. **28**, 523 (1978).
[2] M. Baranger and K. Kumar, Nucl. Phys. **A110**, 410 (1968); K. Kumar and M. Baranger, *ibid.* **A110**, 529 (1968); H. Yadav, H. Toki, and A. Fassler, Phys. Lett. **76B**, 144 (1978); S.B. Khadkikar and C.R. Praharaj, J. Phys. G **6**, 241 (1980).
[3] G.D. Alkhazov *et al.*, Nucl. Phys. **A504**, 549 (1989).
[4] C. Thibault *et al.*, Nucl. Phys. **A367**, 1 (1981).
[5] I.Y. Lee *et al.*, Phys. Rev. Lett. **39**, 682 (1974); M.V. Hoen *et al.*, Phys. Rev. C **24**, 1667 (1981); F.T. Baker, Nucl. Phys. **A331**, 39 (1979).
[6] J.H. Hamilton, P.G. Hansen, and E.F. Zganjar, Rep. Prog. Phys. **48**, 631 (1985); J.H. Hamilton, Nukleonika **24**, 561 (1979).
[7] R. Bengtsson, T. Bengtsson, J. Dudek, G. Leander, W. Nazarewicz, and J. Zhang, Phys. Lett. B **183**, 1 (1987).
[8] J. Sauvage-Letessier, P. Quentin, and H. Flocard, Nucl. Phys. **A370**, 231 (1981).
[9] P. Dabkiewicz *et al.*, Phys. Lett. **82B**, 199 (1979).
[10] M. Cailliau, J. Letessier, H. Flocard, and P. Quentin, Phys. Lett. **46**, 11 (1973).
[11] P. Bonche *et al.*, Nucl. Phys. **A500**, 308 (1989).
[12] P. Bonche, J. Dobaczewski, H. Flocard, P.-H. Heenen, and J. Meyer, Nucl. Phys. **A510**, 466 (1990).
[13] M. Girod, J.P. Delaroche, and J.F. Berger, Phys. Rev. C **38**, 1519 (1988).
[14] P.G. Reinhard, M. Rufa, J. Maruhn, W. Greiner, and J. Friedrich, Z. Phys. A **323**, 13 (1986).
[15] M.M. Sharma and P. Ring, Phys. Rev. C **46**, 1715 (1992).
[16] S.K. Patra and P.K. Panda, Phys. Rev. C **47**, 1514 (1993).
[17] Y.K. Gambhir, P. Ring, and A. Thimet, Ann. Phys. (N.Y.) **198**, 132 (1990).
[18] S.K. Patra and C.R. Praharaj, Phys. Rev. C **44**, 2552 (1991); L.S. Celenza *et al.*, *ibid.* **41**, 1768 (1990); Sara Cruz-barrios *et al.*, *ibid.* **43**, 181 (1991); R.J. Furnstahl and C.E. Price, *ibid.* **40**, 1398 (1989); R.J. Furnstahl, C.E. Price, and G.E. Walker, *ibid.* **36**, 2590 (1987); R. Brockman, *ibid.* **18**, 1510 (1986).
[19] B.D. Serot and J.D. Walecka, Adv. Nucl. Phys. **16**, 1 (1986).
[20] C.J. Horowitz and B.D. Serot, Nucl. Phys. **A368**, 503 (1981).
[21] M. Girod and J.P. Delaroche, Phys. Rev. C **45**, 1420 (1993); F.S. Stephens *et al.*, Phys. Rev. Lett. **64**, 2623 (1990); D. Ye *et al.*, Phys. Rev. C **41**, R13 (1990); Z. Phys. A **335**, 361 (1990); J.A. Becker *et al.*, Phys. Rev. C **41**, R9 (1990); E.F. Moore *et al.*, Phys. Lett. B **258**, 284 (1991); R.R. Chasman, *ibid.* **219**, 227 (1989); J.E. Draper *et al.*, Phys. Rev. C **42**, R1791 (1990).
[22] J. Boguta and A.R. Bodmer, Nucl. Phys. **A292**, 413 (1977).
[23] P. Moeller *et al.*, At. Data Nucl. Data Tables **39**, 225 (1988).
[24] G. Audi and A.H. Wapstra, Nucl. Phys. **A565**, 1 (1993).
[25] M. Guttormsen, Phys. Lett. B **105** 99 (1981).
[26] J. Libert, J.F. Berger, J.P. Delaroche, and M. Girod, Nucl. Phys. **A553**, 523c (1993).
[27] R.C. Lemmon, J.R. Leigh, J.X. Wei, C.R. Morton, D.J. Hinde, J.O. Newton, J.C. Mein, M. Dasgupta, and N. Rowley, Phys. Lett. B **316**, 32 (1993).

[28] A.B. Balantekin, J.R. Bennett, and S. Kuyucak, Phys. Rev. C **49**, 1079 (1994).

[29] Th. Hilberath, St. Becker, G. Bollen, H.-J. Kluge, U. Kroenert, G. Passler, J. Rikovska, R. Wyss, and the ISOLADE Collaboration, Z. Phys. A **342**, 1 (1992).

[30] M. Finger *et al.*, Nucl. Phys. **A188**, 369 (1972); E. Browne, J.M. Browne, J.M. Dairiki, and R.E. Doebler, in *Table of Isotopes*, 7th ed., edited by C.M. Lederer and V.S. Shirley (Wiley, New York, 1978); N. Rud, D. Ward, H.R. Andrews, R.L. Graham, and J.S. Geiger, Phys. Rev. Lett. **31** 1421 (1973); D. Proetel, R.M. Diamond, and F.S. Stephens, Phys. Lett. B **48**, 102 (1974); S.A. Lane and J.X. Saladin, Phys. Rev. **6**, 613 (1972); M.V. Hoehm, E.B. Shera, Y. Yamazaki, and R.M. Steffen, Phys. Rev. Lett. **39**, 1313 (1977); J.E. Glenn, J.R. Pryor, and J.X. Saladin, Phys. Rev. **188**, 1905 (1969); A. Bockish, K. Bharat-Ram, A.M. Kleinfeld, and K.P. Lieb, Z. Phys. A **289**, 231 (1979); **291**, 245 (1979).

[31] *Table of Isotopes* [30].